

Central Lancashire Online Knowledge (CLoK)

Title	Metabotropic action of postsynaptic kainate receptors triggers hippocampal LTP
Type	Article
URL	https://clock.uclan.ac.uk/16925/
DOI	https://doi.org/10.1038/nn.4505
Date	2017
Citation	Petrovic, Milos, Viana da Silva, Silvia, Clement, James P., Vyklicky, Ladislav, Mulle, Christophe, Gonzalez-Gonzalez, Inmaculada M. and Henley, Jeremy M. (2017) Metabotropic action of postsynaptic kainate receptors triggers hippocampal LTP. <i>Nature Neuroscience</i> , 20. pp. 529-539. ISSN 1097-6256
Creators	Petrovic, Milos, Viana da Silva, Silvia, Clement, James P., Vyklicky, Ladislav, Mulle, Christophe, Gonzalez-Gonzalez, Inmaculada M. and Henley, Jeremy M.

It is advisable to refer to the publisher's version if you intend to cite from the work.
<https://doi.org/10.1038/nn.4505>

For information about Research at UCLan please go to <http://www.uclan.ac.uk/research/>

All outputs in CLoK are protected by Intellectual Property Rights law, including Copyright law. Copyright, IPR and Moral Rights for the works on this site are retained by the individual authors and/or other copyright owners. Terms and conditions for use of this material are defined in the <http://clock.uclan.ac.uk/policies/>

1 Metabotropic action of postsynaptic kainate receptors triggers
2 hippocampal LTP
3
4

5 Milos M. Petrovic^{1,3,4,5*}, Silvia Viana da Silva², James P. Clement⁶, Ladislav Vyklicky⁴,
6 Christophe Mulle², Inmaculada M González-González^{1†}, and Jeremy M. Henley^{1†}
7
8
9
10

11 ¹School of Biochemistry, University of Bristol, Bristol, UK

12 ²Interdisciplinary Institute for Neuroscience, University of Bordeaux, Bordeaux, France.

13 ³School of Pharmacy and Biomedical Sciences, University of Central Lancashire, Preston,
14 UK (present address)

15 ⁴Institute of Physiology, Academy of Sciences, Prague, Czech Republic

16 ⁵Institute of Medical Physiology, School of Medicine, University of Belgrade, Serbia

17 ⁶Neuroscience Unit, Jawaharlal Nehru centre for Advanced Scientific Research, Bangalore,
18 India
19
20

21 * Co-corresponding authors

22 † Joint last authors
23

24 Please address correspondence to: JMH (J.M.Henley@bristol.ac.uk), IMG-G
25 (ggonzalezmi@gmail.com) or MMP (mpetrovic@uclan.ac.uk)
26
27
28
29

30 **Abstract**

31 Long-term potentiation (LTP) in the rat hippocampus is the most extensively studied cellular
32 model for learning and memory. Induction of classical LTP involves an NMDA receptor- and
33 calcium-dependent increase in functional synaptic AMPA receptors mediated by enhanced
34 recycling of internalized AMPA receptors back to the postsynaptic membrane. Here we
35 report a novel, physiologically relevant NMDA receptor-independent mechanism that drives
36 increased AMPA receptor recycling and LTP. This pathway requires the metabotropic action
37 of kainate receptors and activation of G-protein, protein kinase C and phospholipase C. Like
38 classical LTP, kainate receptor-dependent LTP recruits recycling endosomes to spines,
39 enhances synaptic recycling of AMPA receptors to increase their surface expression and
40 elicits structural changes in spines, including increased growth and maturation. These data
41 reveal a new and previously unsuspected role for postsynaptic kainate receptors in the
42 induction of functional and structural plasticity in the hippocampus.

43 **Introduction**

44 The precise dynamic regulation of the number, composition and distribution of postsynaptic
45 AMPA receptors (AMPA receptors) is essential for synaptic transmission and plasticity. Classical
46 LTP, which has been characterised extensively in many brain areas, requires the activation
47 of NMDA receptors (NMDARs) ¹. An equivalent NMDAR-dependent LTP can be induced in
48 cultured hippocampal neurons by brief exposure to the NMDAR co-agonist glycine, which
49 elicits the insertion of AMPARs into the postsynaptic membrane and increases miniature
50 excitatory postsynaptic currents (mEPSCs) ².

51 LTP involves both recycling-dependent increases in AMPAR surface expression at the post-
52 synaptic membrane and increases in dendritic spine size ³. Furthermore, stimuli that induce
53 LTP in dispersed hippocampal neuronal cultures promote recycling and recruitment of
54 transferrin receptor-positive recycling endosomes into spines. This repositioning of the
55 endosomal-recycling compartment is critical for activity-dependent changes in spine
56 morphology and provides a mechanistic link between structural and functional plasticity ^{3, 4}.

57 Kainate receptors (KARs) are tetrameric assemblies of combinations of GluK1 – GluK5
58 subunits. They are present at both pre- and postsynaptic membranes where they perform
59 distinct roles in modulating synaptic transmission, neuronal excitability and network activity ⁵,
60 ⁶, and are implicated in processes ranging from neuronal development and differentiation to
61 neurodegeneration and neuronal cell death ^{5, 7}. In addition to direct ionotropic signalling,
62 KARs also signal through the activation of G proteins leading to PKC activation ^{5, 6, 8-10}. Under
63 physiological glutamate release conditions, postsynaptic KAR metabotropic signalling in CA1
64 and CA3 pyramidal neurones inhibits the hyperpolarisation caused by the post-spike
65 potassium current I (sAHP) ¹¹⁻¹⁴.

66 We, and others, have shown previously that transient kainate (KA) stimulation modulates
67 surface expression of KARs ¹⁵⁻¹⁸ via changes in Rab11-dependent recycling within spines ¹⁹.
68 Here, we report that KA induces an NMDAR-independent increase in the synaptic surface
69 expression of functional AMPARs, as well as the structural plasticity via a pathway that
70 requires metabotropic signalling of postsynaptic GluK2-containing KARs and enhanced
71 endosomal vesicle recycling in spines.

72 **Results**

73 **KAR activation increases surface expression of functional synaptic AMPARs.**

74 We first investigated the effects of KA application on AMPAR surface expression in the
75 presence of tetrodotoxin (TTX, 0.5 μ M), GYKI53655 (40 μ M) and L689560 (5 μ M) to
76 suppress activity-dependent glutamate release and prevent activation of AMPARs and
77 NMDARs respectively. Agonist stimulation of KARs (10 μ M KA, 3 min) significantly increased
78 surface expression of both GluA1 and GluA2 AMPAR subunits (Fig. 1A, $p=0.001$ and
79 $p=0.004$, respectively), without altering the total number of AMPARs (Supplementary Fig.1A-
80 B, $p>0.09$). This KAR-induced increase in plasma membrane expressed AMPARs was
81 blocked by the competitive AMPAR/KAR antagonist CNQX (10 μ M; Fig. 1A, $p>0.9$).

82 To define if the KAR-induced increase in AMPAR surface expression occurred at spines, we
83 immuno-labelled surface expressed GluA1 and GluA2 in non-permeabilised neurons (Fig.
84 1B) and calculated the spine/adjacent dendrite ratio. This was increased for both GluA1 and
85 GluA2 following KAR stimulation ($p=0.001$ for GluA1 and $p=0.003$ for GluA2), indicating
86 preferential AMPAR surface expression in spines. Consistent with this, KAR-stimulation
87 increased surface GluA1 and GluA2 colocalisation with the postsynaptic marker PSD95 (Fig.
88 1C, $p<0.001$).

89 The increase in synaptic GluA1 and GluA2 was induced by a brief (3 min) exposure of the
90 cultured hippocampal neurons to all KA concentrations tested, ranging from 500 nM to 20 μ M
91 (Supplementary Fig. 1C-D, $p<0.001$ and $p<0.001$ respectively). We next tested if nanomolar
92 concentrations of KA increased postsynaptic AMPAR-mediated mEPSCs in CA1 pyramidal
93 neurons in hippocampal slices. KA concentrations below 3 μ M do not activate AMPARs in
94 CA1 ²⁰, but, to fully exclude direct KA activation of AMPARs, we co-applied the AMPAR
95 specific antagonist GYKI53655 (40 μ M) during the transient KA application. GYKI53655 was
96 then washed out to obtain AMPAR mEPSCs. Co-application of GYKI53655 with 500 nM KA
97 did not change mEPSC frequency (Supplementary Fig. 2A, $p>0.3$) but caused a marked
98 increase in the amplitude of mEPSCs (Fig. 1D and Supplementary Fig. 3A, $p<0.004$. These
99 data demonstrate a KAR-induced increase of functional postsynaptic AMPARs.

100 **KAR-mediated NMDAR-independent LTP.**

101 Increased postsynaptic AMPARs surface expression underpins LTP, so we investigated the
102 effects of KAR activation on synaptically evoked AMPAR-mediated excitatory postsynaptic
103 responses in rat hippocampal slices. KA (10 μ M, 3 min) caused a transient depression
104 followed by a progressive increase in AMPAR-mediated CA1 EPSCs (Supplementary Fig.
105 4A; $169.8\% \pm 31.4\%$, $p=0.01$) with no change in glutamate release probability determined by
106 the paired-pulse ratio (PPR; Supplementary Fig. 4B) in the continuous presence of 100 μ M
107 APV (to block NMDARs). At this concentration, however, KA activates AMPARs and could
108 affect their dynamics. Thus, we performed the experiment as above, but using 40 μ M
109 GYKI53655 (present prior to and during KA application to block AMPARs). Although in the
110 presence of GYKI53655 there was a significant difference in amplitude between the control
111 and KA conditions (KA, $100.8\% \pm 15.5\%$; Control $54.6\% \pm 8.0\%$, $p=0.009$; Supplementary
112 Fig. 4C, unchanged PPRs are shown in Supplementary Fig. 4D and representative
113 responses shown in Supplementary Fig. 4E), GYKI53655 masked the time course of
114 AMPAR-mediated EPSCs. We therefore reduced the KA concentration to 500 nM, thereby
115 avoiding the need to block AMPARs with GYKI53655. Under these conditions, 500 nM KA
116 caused a progressive and persistent increase in AMPAR-mediated CA1 EPSCs (Figure 2A;
117 $133.1\% \pm 11.4\%$, $p=0.02$), reaching a peak approximately 10-15 min after the agonist
118 application. Again, we found no change in PPR (Supplementary Fig. 4F, $p>0.3$). Combined
119 with our mEPSC data, these evoked EPSC results indicate that KAR activation elicits
120 NMDAR-independent KA-induced LTP via increased surface expression of postsynaptic
121 AMPARs in CA1 hippocampal neurons.

122 Consistent with this, KA did not induce any potentiation in AMPAR-mediated field potentials
123 in the CA1 region of hippocampal slices from GluK2-knockout (GluK2^{-/-}) mice ($95.7 \pm 3.6\%$,
124 $p > 0.05$, Supplementary Fig 5A). To exclude any possible developmental effects in the
125 GluK2-knockout mice, we tested the effect of acutely blocking KARs in wild-type mice using
126 the AMPAR/KAR blocker CNQX (10 μ M) prior to and during KA challenge, followed by
127 CNQX washout (Supplementary Fig. 5B). Compared to sham controls (CNQX only), the
128 recovery profile was unchanged ($80.2 \pm 3.4\%$ vs. $78.7 \pm 9.5\%$ for KA and control, $p > 0.05$).
129 We also confirmed that KA application potentiated AMPAR responses in hippocampal slices
130 obtained from adult, 3-month old mice ($124.7 \pm 9.6\%$, $p < 0.01$) (Supplementary Fig. 5C-D),
131 indicating that KA-induced LTP is not developmentally restricted.

132 Using wild-type and GluK2-knockout mice, we next examined the KAR dependency of a
133 previously reported NMDAR-independent form of LTP evoked by high frequency stimulation
134 (HFS) protocol, based on the modified procedure from ^{21, 22} (illustrated in schematic form in
135 Fig. 2B and described in Methods). As shown in Supplementary Fig. 6A-C, field potential
136 recordings revealed robust LTP in acute hippocampal slices from wild-type mice ($185.8 \pm$

137 26.1% vs. $106.1 \pm 5.2\%$ in test vs. control pathway, $p=0.007$), whereas a reduced LTP was
138 obtained in GluK2-knockout mice ($170.3 \pm 17.3\%$ vs. $106.2 \pm 5.7\%$ in test vs. control
139 pathway, $p=0.03$). To isolate the NMDAR-independent component of this LTP, we used 50
140 μM D-APV, which completely blocked LTP in the GluK2-knockout ($106.3 \pm 5.0\%$ vs. $99.4 \pm$
141 4.6% in test vs. control pathway, $p>0.5$), but not in WT mice ($128.5 \pm 11.4\%$ vs. $107.7 \pm 5.0\%$
142 in test vs. control pathway, $p<0.02$). No changes in PPR were observed (Supplementary Fig.
143 6D). These data confirm that activation of GluK2-containing KARs by synaptically released
144 glutamate induces NMDAR-independent and KAR-dependent hippocampal LTP.

145 Consistent with previous reports²², the NMDAR-independent component of this HFS LTP in
146 wild-type mice was blocked by the L-type calcium blocker nifedipine ($110.45 \pm 3.66\%$ vs.
147 $104.05 \pm 3.81\%$, $p>0.05$, test vs. control pathway, Supplementary Fig. 7A). As in previous
148 experiments, no change in the PPR was detected (Supplementary Fig. 7B).

149 Although widely used, HFS does not correspond to intrinsic *in vivo* patterns of hippocampal
150 activity. Therefore, to determine if KAR-dependent LTP can be induced by more
151 physiological stimuli, we used a protocol based on hippocampal sharp-wave/ripple-like
152 stimulation pattern (RL-LTP; illustrated in schematic form in Fig. 2C)²³. In wild-type mice, the
153 RL-LTP protocol resulted in a progressive potentiation that peaked 10-15 min after
154 stimulation (Fig. 2D left panel; $166.2 \pm 8.5\%$ vs. $101.1 \pm 2.9\%$ in test vs control pathway,
155 $p<0.001$). In GluK2-knockout mice (Fig. 2D right panel; representative traces in Fig. 2E),
156 there was a significantly reduced LTP ($139.7 \pm 7.5\%$ vs. $100.6 \pm 2.7\%$ in test vs. control
157 pathway, $p<0.001$, and $p=0.03$ compared to wild-type mice, Fig. 2F). Importantly, however,
158 while RL-LTP (although at reduced level) was still detected in wild-type mice in the presence
159 of 50 μM D-APV (Fig 2D left panel; $120.9 \pm 2.3\%$ vs. $99.5 \pm 2.8\%$ in test vs control pathway,
160 $p<0.001$), RL-LTP was completely prevented in GluK2-knockout mice ($99.1 \pm 4.0\%$ vs. $99.2 \pm$
161 3.8% , test vs control pathway, $p=0.98$, and $p=0.002$ compared to wild-type mice).

162 D-APV is a competitive antagonist, therefore, to exclude the theoretical possibility that the
163 intense RL-LTP stimulation paradigm could lead to glutamate accumulation in synaptic cleft
164 that could out-compete D-APV, thereby allowing NMDAR-dependent LTP, we used a
165 previously described strategy²⁴. We first blocked the NMDARs with MK-801 (20 μM), a use-
166 dependent blocker (in nominal 0 mM Mg^{2+} aCSF, to facilitate the NMDAR activation). Then,
167 once the full blockade was achieved, we reintroduced ordinary aCSF, continuously
168 supplemented with MK-801 (20 μM) and D-AP5 (50 μM). Robust potentiation still occurred in
169 wild-type mice, further confirming the KAR-dependent component of RL-LTP (142.6 ± 0.6 vs.
170 $98.2 \pm 9.3\%$ in test vs. control pathway, $p<0.01$; Supplementary Fig. 7C-D).

171 Finally, to further discount any possible confounding developmental issues in GluK2-
172 knockout mice, we performed the RL-LTP experiment in wild-type mice while acutely
173 blocking KARs using CNQX (10 μ M, present prior to and during LTP induction, followed by
174 washout), similarly to the approach used in Supplementary Fig. 5B. No RL-LTP was induced
175 after full inhibition by CNQX, *i.e.* both test and control pathways gradually recovered with
176 similar temporal profiles (Supplementary Fig. 7E, minutes 37-41: 20.9 ± 4.6 % vs. 22.3 ± 3.2 ,
177 $p > 0.05$; minutes 57-61: 75.1 ± 6.00 % vs. 70.9 ± 6.46 %, $p > 0.05$; minutes 77-81: $100.4 \pm$
178 0.7 % vs. 100.5 ± 2.6 %, $p > 0.05$, test vs. control pathway). These results provide
179 compelling evidence that physiologically relevant stimulation of GluK2-containing KARs can
180 induce NMDAR-independent LTP in the hippocampus.

181 Next, using rat hippocampal slices, we performed within-slice comparisons of test and control
182 pathway responses to RL-LTP and KA application. First we induced RL-LTP (normalized
183 fEPSP slope in test and control pathway = 123.1 ± 1.8 % and 98.1 ± 1.6 %, respectively,
184 $p < 0.001$, Supplementary Fig. 8A-C). We then subjected the slice to bath application of KA
185 (500 nM, 3 min), which caused a robust increase in control pathway to levels equivalent to
186 the RL-LTP in the test pathway (normalized fEPSP slope in test and control pathway = 132.9
187 ± 2.4 % and 131.7 ± 3.6 %, respectively; $p = 0.78$). Importantly, however, there was no further
188 increase in the pathway previously subjected to RL-LTP. These data also demonstrate that
189 the extent of agonist-induced LTP in field recordings is comparable to that achieved by
190 patch-clamp recording.

191 Our data from GluK2^{-/-} mice indicate that LTP is not saturated in the presence of D-APV
192 because RL-LTP induced significantly stronger LTP in WT mice. In a complementary
193 approach, we directly tested if agonist and electrical stimulation-induced KAR-LTP share a
194 common mechanism using a previously established occlusion protocol²⁵.

195 We initially induced RL-LTP in one pathway (black circles, Supplementary Fig. 8D, $100.9 \pm$
196 2.05 % vs. 133.4 ± 10.00 %, $p < 0.05$) and then bath applied KA (500 nM, 3 min). As expected,
197 and consistent with the data in Supplementary Fig. 8A, the pathway that had not been
198 subjected to RL-LTP was potentiated by kainate (white circles, Supplementary Fig. 8D-E,
199 118.1 ± 4.0 %, $p < 0.01$). Importantly, KA did not cause additional potentiation in the pathway
200 previously exposed to RL-LTP (black circles, 128.0 ± 11.2 %, $p > 0.05$). The stimulation
201 intensity of the *test* pathway (white circles) was then adjusted to normalise it to its basal level
202 (101.6 ± 5.7 %, $p > 0.05$) and the RL-LTP protocol was then delivered to this pathway
203 (Supplementary Fig. 8D-E). Since no further potentiation was observed (97.6 ± 9.3 %, $p >$
204 0.05), this inverse occlusion experiment confirms that KA-induced potentiation and RL-LTP
205 share a common mechanism.

206 **KAR activation induces structural plasticity via enhanced endosomal recycling.**

207 NMDAR-dependent LTP elicits structural changes in spine shape and increased spine size ⁴.
208 Correspondingly, transient KA application robustly increases spine density and maturity (Fig.
209 3A-C), More specifically, there are increases in mature spine size (65.1% ± 14%, p<0.001;
210 Fig. 3A) and numbers of dendritic protrusions (68.9% ± 25%, p<0.001; Fig. 3B), as well as
211 enhanced transition from stubby to mushroom spines (18.7% ± 4%, p<0.001; Fig. 3C).

212 NMDAR-dependent LTP also enhances generalised endosomal recycling of cargo proteins
213 and membrane within the spine ^{3, 4}. To investigate if the same mechanisms underlie KAR-
214 dependent LTP, we monitored transferrin-Alexa594 (Tf-A594) labelled recycling endosomes.
215 Tf-A594 endosomes distribute mainly at the base of spines in non-stimulated control
216 neurons. Following transient KA application, however, Tf-A594 endosomes translocate from
217 the dendritic shaft to the spine head (Fig. 4A). Furthermore, expression of a dominant
218 negative version of the recycling endosome-associated small GTPase Rab11 (Rab11dn),
219 which blocks NMDAR-dependent LTP ²⁶, prevented the KAR-evoked recruitment of recycling
220 endosomes into spines (Fig. 4B) and blocked the increases in the head diameter of
221 mushrooms spines (p<0.0001 for KA - control, and Rab11wt - Rab11dn; Fig. 4C).

222 To confirm the role of recycling in KAR-dependent LTP, we used surface biotinylation assays
223 in combination with primaquine to selectively inhibit recycling ²⁷ or monensin to block both
224 recycling and lysosomal degradation ²⁸. As expected, both drugs prevented the KAR-induced
225 increase in GluA1 and GluA2 surface expression (Supplementary Fig. 9A-B, p<0.001). We
226 next quantified surface expression of GluA1 and GluA2 in spines and adjacent shaft regions.
227 Inhibiting recycling with primaquine, monensine or Rab11dn prevented the KAR-induced
228 change in the spine:dendrite ratio of AMPAR surface expression (Supplementary Fig. 10A-C,
229 p=0.18 for GluA1 and p=0.24 for GluA2, p=0.80 GluA1 and p=0.34 GluA2, and p=0.03 for
230 GluA1 and p=0.02 for GluA2). These data indicate that both NMDAR- and KAR-dependent
231 LTP require the recruitment and enhanced recycling of endosomal vesicles in spines.

232 **KAR-dependent LTP is mediated via a non-canonical G-protein-associated signalling**
233 **pathway.**

234 Although some mechanistic details are still lacking, it is now clear that KARs signal via G-
235 protein-dependent pathways to increase intracellular calcium [Ca²⁺]_i, and activate protein
236 kinase C (PKC) and phospholipase C (PLC) ^{5, 6, 9, 10, 29}. Since increased [Ca²⁺]_i is required for
237 LTP, ^{30, 31} we tested the source of [Ca²⁺]_i increase in KAR-dependent LTP using the
238 extracellular chelator EDTA and the membrane permeant chelator BAPTA-AM. The
239 presence of BAPTA-AM, but not EDTA, during the KA application blocked the KAR-evoked
240 increase in synaptic AMPAR surface expression (Fig. 5A, B; controls without KA shown in

241 **Supplementary Fig. 11A**; BAPTA-AM; GluA1, $p=0.5$; GluA2 $p=0.10$; EDTA; GluA1 $p=0.009$;
242 GluA2 $p<0.001$) and the associated changes in the structural plasticity (**Fig. 5C** and
243 **Supplementary Fig. 11B**, EDTA; $p<0.001$; BAPTA-AM $p=0.61$). Similarly, preincubation with
244 PKC inhibitor chelerythrine or the PLC inhibitor U73122 blocked the KAR-induced increase in
245 GluA1 and GluA2 expression at synapses (**Fig. 5A, B**; controls without KA shown in
246 **Supplementary Fig. 11A-B**; U73122: GluA1 $p=0.56$; GluA2 $p=0.32$; chelerythrine: GluA1
247 $p=0.54$, GluA2 $p=0.78$), the increase in the spine size (**Fig. 5C** and **Supplementary Fig. 11B**,
248 U73122: $p=0.42$; chelerythrine: $p=0.48$), as well as the agonist-evoked KAR-dependent LTP
249 in electrophysiological recordings ($100.5 \pm 1.4\%$, $p>0.05$ for U73122 and $100.7 \pm 5.8\%$,
250 $p>0.05$ for chelerythrine, **Fig. 5D, E**).

251 We also analysed PKC and PLC activity in cells after triggering KAR-dependent LTP. Brief
252 KAR stimulation (3 min, 500nM) elicited a nearly 2-fold increase in PLC and PKC activity
253 compared to unstimulated cells (**Fig. 5F**). Furthermore, the extent of PKC activation in KAR-
254 dependent LTP is similar to stimulation by the phorbol ester PMA (0.5 μ M, 3min, $p=0.4$). The
255 KAR-induced activation of PKC and PLC was prevented by CNQX and BAPTA-AM, but not
256 by the presence of EDTA during KA application (**Fig. 5F**: PKC: +CNQX: $p=0.037$, +EDTA:
257 $p=0.81$, +BAPTA-AM, $p=0.002$, +Chelerythrine $p=0.038$. For PLC: +CNQX: $p=0.047$, +EDTA:
258 $p=0.84$, +BAPTA-AM: $p=0.056$, +U73122 $p=0.006$). Finally, in addition to EGTA (5 mM)
259 application only during KA application, we continuously applied (30 min during and after KA
260 application) the selective Ca^{2+} chelator EGTA to bind extracellular Ca^{2+} or nifedipine to block
261 L-type voltage-gated Ca^{2+} channels (VGCCs). Continuous application of either drug
262 prevented the KA-induced increase in GluA1 and GluA2 surface expression at synapses
263 (**Supplementary Fig. 11C, D**; $p<0.001$), suggesting a delayed role for extracellular Ca^{2+} in
264 KAR-LTP. Importantly, inhibiting Group I /II metabotropic glutamate receptors with the
265 specific antagonist MCPG did not affect KAR-dependent increases in synaptic AMPARs or
266 spine size. (**Supplementary Fig. 12A, B**; $p<0.001$ and $p=0.018$). These data demonstrate that
267 KAR-LTP requires activation of PKC and PLC and intracellular calcium release, consistent
268 with a KAR-mediated metabotropic signalling pathway.

269 Furthermore, we performed the same experiments as those shown in **Figure 1C**, but with the
270 preincubation in the presence of G-protein inhibitor pertussis toxin (PTX) (1 μ g/mL, 1 hour).
271 PTX prevented KA-induced activation of both PLC and PKC (**Fig. 6A**, $p=0.03$ and $p=0.012$
272 respectively). PTX also blocked the increased colocalization of GluA1 and GluA2 with PSD95
273 following the KA challenge (**Fig. 6B**, GluA1, $p=0.93$; GluA2 $p=0.47$, compare with **Fig. 1C**).
274 Furthermore, incubation of hippocampal slices with PTX prior to recording mEPSCs
275 prevented the KAR-induced increase in AMPAR mEPSC amplitude in CA1 pyramidal
276 neurons (**Fig. 6C**, $p=0.34$, compare with **Fig. 1D**), with no change in the frequency

277 (Supplementary Fig. 13A $p > 0.1$). Correspondingly, agonist-evoked and electrically stimulated
278 KAR-dependent LTP (Fig. 6D-E and Supplementary Fig. 13B-D, $p = 0.69$ and $p = 0.3$, compare
279 with Fig. 2A), as well as structural plasticity (Fig. 6F and Supplementary Fig. 13E, $p = 0.4$,
280 compare with Fig. 3A) were prevented by preincubation with PTX, again indicating the
281 requirement for a metabotropic action for KARs.

282 Both our imaging and functional data using nifedipine suggest that following initial LTP
283 induction that requires intracellular Ca^{2+} , extracellular calcium entry through L-type VGCCs
284 plays a role in maintaining KAR-LTP. Moreover, VGCC currents can be modulated by G-
285 protein activation³². We therefore used patch-clamp electrophysiology to measure VGCC
286 Ca^{2+} currents. KA application (500 nM, 3 min) increased VGCC currents in control conditions
287 ($127.4 \pm 16.1\%$, $n = 5$), but there was no increase in slices that had been preincubated with
288 PTX ($90.4 \pm 4.5\%$, $n = 4$, $p < 0.05$, Supplementary Fig. 14).

289 Substitution of extracellular Na^+ with an equimolar concentration of the non-permeant cation
290 N-methyl-D-glucamine (NMDG) prevents KAR channel conductance, but does not impede
291 metabotropic KAR activity⁹. Replacing Na^+ with NMDG does not block the KAR-induced
292 increase in GluA1 and GluA2 colocalization with PSD95 and spine size (Supplementary
293 Fig.15A-B; GluA1, $p = 0.004$, GluA2, $p < 0.001$ and $p = 0.009$ for spine size), further confirming
294 that ionotropic activity is not required for KAR-dependent LTP. The KAR antagonist UBP310
295 has been reported to inhibit KAR ionotropic activity, but not KAR-metabotropic signalling, via
296 a mechanism that likely involves an action beyond simple competitive antagonism³³. This
297 effect is unlikely to be due to different subunit compositions since most KARs in the brain
298 comprise GluK2/5 combinations. We anticipate that future studies will uncover the
299 mechanisms underlying this selective inhibition of ionotropic over metabotropic KAR activity.
300 Nonetheless, consistent with the documented selectively ionotropic action, UBP310 (10 μ M)
301 did not block KA-induced increases in PLC and PKC activity (Fig. 7A, $p = 0.74$ and $p = 0.94$
302 compared to KA) nor did it prevent KAR-dependent LTP (Fig. 7B-C and Supplementary
303 Fig.15C-D $p = 0.01$ and $p = 0.006$) and structural spine plasticity (Fig.7D, $p = 0.03$).

304 Taken together, this array of complementary and mutually supportive data provide
305 compelling evidence that KAR channel activity is not required for KAR-dependent LTP, but is
306 instead underpinned by KAR-mediated metabotropic signalling.

307 Discussion

308 Here we report that KAR activation can elicit a previously unanticipated form of NMDAR-
309 independent LTP. This occurs via a metabotropic KAR pathway that recruits endosomal
310 recycling machinery from the dendritic shaft into the spine to alter post-endocytic GluA1 and
311 GluA2 sorting and exocytosis back to the spine plasma membrane.

312 **KAR activation increases AMPAR surface expression at postsynapse**

313 We have shown previously that transient KA application can increase KAR surface
314 expression ¹⁶ and enhance spine growth by altering post-endocytic sorting and enhanced
315 recycling mechanisms ¹⁹. Furthermore, KARs regulate neurite outgrowth ^{16, 34, 35}, as well as
316 filopodia and nascent spinule development ³⁶. Here we show that transient KAR activation
317 augments recycling and surface expression of AMPARs, increases AMPAR colocalisation
318 with PSD95 in spines and increases the amplitude of AMPAR mEPSCs. Consistent with
319 postsynaptic mechanisms, the probability of neurotransmitter release was unchanged.
320 Furthermore, using two different stimulation protocols, we demonstrate that synaptic
321 activation of GluK2-containing KARs underlies the increases in the evoked AMPAR-mediated
322 responses. These results reveal a novel and physiologically relevant form of postsynaptic
323 KAR-dependent, NMDAR-independent LTP.

324 **KAR activation increases synaptic recycling and spine size**

325 In parallel with increased AMPAR-mediated neurotransmission, NMDAR-dependent LTP
326 elicits the formation and enlargement of dendritic spines to consolidate neural circuitry ^{37, 38}.
327 Recycling endosomes are recruited to deliver membrane material directly within spines for
328 structural plasticity ^{3, 4}, providing a mechanistic link for coupling changes in spine size to the
329 regulation of AMPAR-mediated transmission and LTP ³⁹. Like NMDAR-dependent LTP, KAR-
330 dependent LTP requires translocation of Rab11-positive recycling endosomes from the
331 dendritic shaft into spines. Moreover, overexpression of dominant negative Rab11, which
332 blocks NMDAR-dependent LTP ⁴⁰, prevents the KAR-evoked redistribution of recycling
333 endosomes to spines and blocks KAR-dependent LTP. This involvement of Rab11 in
334 NMDAR-dependent and KAR-dependent LTP indicates shared mechanisms in both
335 pathways.

336 **Metabotropic actions of KARs mediate KAR-dependent LTP**

337 Metabotropic KAR signalling was first identified through the KAR-mediated modulation of
338 GABA release, which does not require KAR channel activation, but is prevented by inhibition
339 of G-protein and PKC activity ⁸. Subsequently, KAR-dependent inhibition of the slow after-
340 hyperpolarizing potential (sAHP), which enhances neuronal excitability, was also shown to
341 be mediated by metabotropic KAR signalling ¹¹. Although there is now a wealth of
342 experimental support for metabotropic action of both pre- and postsynaptic KARs (for
343 reviews see ^{5, 6, 41}), many questions remain. For example, the identity of the KAR subunit
344 conferring metabotropic action is unclear because the literature is contradictory and no KAR
345 subunits contain conventional G-protein binding motifs. Nonetheless, it is now generally
346 accepted that metabotropic KAR signalling is PTX sensitive and thus involves Go rather than

347 Gq protein activation. Accordingly, a recent report has suggested that the KAR subunit
348 GluK1 can associate directly with a Go protein α subunit and that this association is
349 responsible for the metabotropic effects of KARs¹⁰. Our results now reveal an entirely novel
350 role for metabotropic KAR signalling in regulating AMPAR trafficking, spine morphology and
351 NMDAR-independent LTP.

352 **KAR-dependent LTP**

353 LTP at CA1 hippocampal synapses is not uniform and comprises a range of NMDAR-
354 dependent and -independent plasticity mechanisms⁴². Given the crucial importance of
355 plastic changes in the brain, this array of pathways provides a dynamic, flexible and reliable
356 system to ensure the continuity of neuronal network and brain function. Our identification of a
357 novel postsynaptic KAR-dependent LTP adds to these important system traits. Ripple-like
358 high-frequency patterns of activity (~200 Hz for ~100 ms, repeating at ~1 Hz) occur in
359 immobile awake animals and during slow wave sleep⁴³. These patterns generally occur in
360 conjunction with large-amplitude sharp waves and ripple-related activity *in vivo* is implicated
361 in LTP that underlies memory consolidation in the hippocampus^{44, 45}. Here, we show for the
362 first time that this strong and physiologically relevant ripple-like activity LTP induction
363 protocol (RL-LTP) is mediated via GluK2-containing KARs.

364 It is notable that the induction of KAR-LTP and the previously reported agonist-evoked
365 increase in surface expression of GluK2-containing KARs share a similar time course that
366 reaches a plateau 10-15 min after stimulation¹⁶. This profile correlates with the delayed
367 NMDAR-independent component of HFS-induced LTP²¹ and shares dependency on VGCC
368 activation. Moreover, G-protein potentiation of VGCC activity is sensitive to PTX and requires
369 PKC activation and increases in $[Ca^{2+}]_i$ ³², consistent with KAR-metabotropic actions
370 modulating VGCC activity in NMDAR-independent LTP. These features are similar to the role
371 of mGluR5 receptor metabotropic signalling which, by facilitating L-type VGCC activity via
372 intracellular Ca^{2+} release, contributes to NMDAR-independent forms of LTP⁴⁶. It is important
373 to note that the rise in $[Ca^{2+}]_i$, presumably mediated via IP3 receptors, can facilitate VGCC
374 activity and that VGCC activity and the influx of extracellular calcium can prolong the
375 temporal profile and frequency of intracellular Ca^{2+} -release events⁴⁷. This reciprocal
376 feedback system fits with our imaging and electrophysiological experiments with nifedipine
377 and can extend beyond the kainate stimulation. We anticipate that future work will explore
378 this feedback system in more detail by combining simultaneous multiphoton imaging and
379 electrophysiology in brain slices.

380 **Concluding remarks**

381 Here we describe an entirely new pathway in which direct activation of postsynaptic KARs
382 induces LTP. These data show that KAR metabotropic signalling facilitates information
383 transfer and synaptic integration by two parallel mechanisms, namely the short-term
384 regulation of excitability ^{13, 14} and long term increase in synaptic efficacy via LTP. Both
385 mechanisms are induced by high frequency stimulation of KARs and require PKC. Given that
386 KARs are highly expressed during the neuronal circuit formation, and that their dysfunction is
387 implicated in many neurological diseases including epilepsy ⁴⁸ and intellectual disability ⁴⁹,
388 we anticipate that our findings will have far reaching implications.

389 **Acknowledgements**

390 We are grateful for financial support from the ERC (Proposal n° 232881), MRC
391 (MR/L003791), BHF (PG/14/60/31014) and BBSRC (BB/K014366 and BB/K014358) to JMH;
392 EMBO Fellowships to MIGG (ALTF 224-2009 and ASTF 438-2011) and MMP (ASTF 232-
393 2011); MRC (MR/M023729/1) to MMP; the Centre National de la Recherche Scientifique, the
394 Conseil Régional d'Aquitaine, the Labex BRAIN and the Fundacao para a Ciencia e a
395 Tecnologia to CM and SVS; the Czech Science Foundation (GACR): 17-02300S;
396 P304/12/G069) and Research Project of the AS CR RVO (67985823) to LV; the Department
397 of Science and Technology (DST) – Young Scientist Scheme (SERB/LS-779/2013) to JPC.
398 We are grateful to P. Rubin and N. Grosjean for excellent technical support, A. Singh for his
399 help in some follow-up experiments and to J. Esteban (CBMSO, Madrid) for providing Rab
400 constructs.

401 **Author contributions**

402 MIGG designed and performed the biochemistry and imaging experiments and participated
403 in electrophysiological experiments; MMP designed and performed agonist and stimulation
404 evoked electrophysiology and participated in imaging experiments. SVS did
405 electrophysiology in wild-type and GluK2^{-/-} mice hippocampal slices; CM provided knockout
406 mice and extensive advice; JPC performed the MK-801/D-APV and CNQX dual pathway
407 electrophysiological experiments. LV provided facilities and reagents and helped analyse the
408 electrophysiological data. JMH instigated the study and provided overall supervision and
409 management. JMH, MIGG and MMP designed the study, analysed the data and wrote the
410 paper. All authors discussed the results and commented on the manuscript.

411 **Author Information**

412 The authors declare no competing financial interests.

413

414 **References**

- 415 1. Malenka, R.C. & Bear, M.F. LTP and LTD: an embarrassment of riches. *Neuron* **44**, 5-
416 21 (2004).
- 417 2. Lu, W., *et al.* Activation of synaptic NMDA receptors induces membrane insertion of
418 new AMPA receptors and LTP in cultured hippocampal neurons. *Neuron* **29**, 243-254.
419 (2001).
- 420 3. Park, M., Penick, E.C., Edwards, J.G., Kauer, J.A. & Ehlers, M.D. Recycling
421 endosomes supply AMPA receptors for LTP. *Science* **305**, 1972-1975 (2004).
- 422 4. Park, M., *et al.* Plasticity-induced growth of dendritic spines by exocytic trafficking from
423 recycling endosomes. *Neuron* **52**, 817-830 (2006).
- 424 5. Contractor, A., Mulle, C. & Swanson, G.T. Kainate receptors coming of age: milestones
425 of two decades of research. *Trends Neurosci* **34**, 154-163 (2011).
- 426 6. Lerma, J. & Marques, J.M. Kainate receptors in health and disease. *Neuron* **80**, 292-
427 311 (2013).
- 428 7. González-González, I.M., *et al.* Kainate Receptor Trafficking. *WIREs Membrane*
429 *Transport and Signalling* **1**, 31-44 (2012).
- 430 8. Rodriguez-Moreno, A. & Lerma, J. Kainate receptor modulation of GABA release
431 involves a metabotropic function. *Neuron* **20**, 1211-1218. (1998).
- 432 9. Rozas, J.L., Paternain, A.V. & Lerma, J. Noncanonical signaling by ionotropic kainate
433 receptors. *Neuron* **39**, 543-553 (2003).
- 434 10. Rutkowska-Wlodarczyk, I., *et al.* A Proteomic Analysis Reveals the Interaction of
435 GluK1 Ionotropic Kainate Receptor Subunits with Go Proteins. *J Neurosci* **35**, 5171-
436 5179 (2015).
- 437 11. Melyan, Z., Wheal, H.V. & Lancaster, B. Metabotropic-mediated kainate receptor
438 regulation of IsAHP and excitability in pyramidal cells. *Neuron* **34**, 107-114 (2002).
- 439 12. Fisahn, A., Heinemann, S. & McBain, C.J. The Kainate Receptor Subunit GluR6
440 Mediates Metabotropic Regulation of the Slow and Medium AHP Currents in Mouse
441 Hippocampal Neurons. *J Physiol* (2004).
- 442 13. Melyan, Z., Lancaster, B. & Wheal, H.V. Metabotropic regulation of intrinsic excitability
443 by synaptic activation of kainate receptors. *J Neurosci* **24**, 4530-4534 (2004).
- 444 14. Ruiz, A., Sachidhanandam, S., Utvik, J.K., Coussen, F. & Mulle, C. Distinct subunits in
445 heteromeric kainate receptors mediate ionotropic and metabotropic function at
446 hippocampal mossy fiber synapses. *J Neurosci* **25**, 11710-11718 (2005).
- 447 15. Rivera, R., Rozas, J.L. & Lerma, J. PKC-dependent autoregulation of membrane
448 kainate receptors. *EMBO J* **26**, 4359-4367 (2007).

- 449 16. Martin, S., Bouschet, T., Jenkins, E.L., Nishimune, A. & Henley, J.M. Bidirectional
450 regulation of kainate receptor surface expression in hippocampal neurons. *J Biol Chem*
451 **283**, 36435-36440 (2008).
- 452 17. Selak, S., *et al.* A role for SNAP25 in internalization of kainate receptors and synaptic
453 plasticity. *Neuron* **63**, 357-371 (2009).
- 454 18. Carta, M., *et al.* CaMKII-dependent phosphorylation of GluK5 mediates plasticity of
455 kainate receptors. *EMBO J* **32**, 496-510 (2013).
- 456 19. Gonzalez-Gonzalez, I.M. & Henley, J.M. Postsynaptic Kainate Receptor Recycling and
457 Surface Expression Are Regulated by Metabotropic Autoreceptor Signalling. *Traffic*
458 (2013).
- 459 20. Bureau, I., Bischoff, S., Heinemann, S.F. & Mulle, C. Kainate receptor-mediated
460 responses in the CA1 field of wild-type and GluR6-deficient mice. *J Neurosci* **19**, 653-
461 663 (1999).
- 462 21. Grover, L.M. & Teyler, T.J. Normal-Methyl-D-Aspartate Receptor-Independent Long-
463 Term Potentiation in Area CA1 of Rat Hippocampus - Input-Specific Induction and
464 Preclusion in a Non-Tetanized Pathway. *Neuroscience* **49**, 7-11 (1992).
- 465 22. Grover, L.M. & Teyler, T.J. Two components of long-term potentiation induced by
466 different patterns of afferent activation. *Nature* **347**, 477-479 (1990).
- 467 23. Behrens, C.J., van den Boom, L.P., de Hoz, L., Friedman, A. & Heinemann, U.
468 Induction of sharp wave-ripple complexes in vitro and reorganization of hippocampal
469 networks. *Nat Neurosci* **8**, 1560-1567 (2005).
- 470 24. Grover, L.M. Evidence for postsynaptic induction and expression of NMDA receptor
471 independent LTP. *J Neurophysiol* **79**, 1167-1182 (1998).
- 472 25. Huang, Y.Y. & Malenka, R.C. Examination of TEA-induced synaptic enhancement in
473 area CA1 of the hippocampus: the role of voltage-dependent Ca²⁺ channels in the
474 induction of LTP. *J Neurosci* **13**, 568-576 (1993).
- 475 26. Brown, T.C., Correia, S.S., Petrok, C.N. & Esteban, J.A. Functional
476 compartmentalization of endosomal trafficking for the synaptic delivery of AMPA
477 receptors during long-term potentiation. *J Neurosci* **27**, 13311-13315 (2007).
- 478 27. van Weert, A.W., Geuze, H.J., Groothuis, B. & Stoorvogel, W. Primaquine interferes
479 with membrane recycling from endosomes to the plasma membrane through a direct
480 interaction with endosomes which does not involve neutralisation of endosomal pH nor
481 osmotic swelling of endosomes. *European journal of cell biology* **79**, 394-399 (2000).
- 482 28. Mollenhauer, H.H., James Morr e, D. & Rowe, L.D. Alteration of intracellular traffic by
483 monensin; mechanism, specificity and relationship to toxicity. *Biochimica et Biophysica*
484 *Acta (BBA) - Reviews on Biomembranes* **1031**, 225-246 (1990).

- 485 29. Sihra, T.S., Flores, G. & Rodriguez-Moreno, A. Kainate Receptors: Multiple Roles in
486 Neuronal Plasticity. *Neuroscientist* (2013).
- 487 30. Lynch, G., Larson, J., Kelso, S., Barrionuevo, G. & Schottler, F. Intracellular injections
488 of EGTA block induction of hippocampal long-term potentiation. *Nature* **305**, 719-721
489 (1983).
- 490 31. Malenka, R.C., Kauer, J.A., Zucker, R.S. & Nicoll, R.A. Postsynaptic calcium is
491 sufficient for potentiation of hippocampal synaptic transmission. *Science* **242**, 81-84
492 (1988).
- 493 32. Zong, X. & Lux, H.D. Augmentation of calcium channel currents in response to G
494 protein activation by GTP gamma S in chick sensory neurons. *J Neurosci* **14**, 4847-
495 4853 (1994).
- 496 33. Pinheiro, P.S., *et al.* Selective block of postsynaptic kainate receptors reveals their
497 function at hippocampal mossy fiber synapses. *Cereb Cortex* **23**, 323-331 (2013).
- 498 34. Marques, J.M., *et al.* CRMP2 tethers kainate receptor activity to cytoskeleton dynamics
499 during neuronal maturation. *J Neurosci* **33**, 18298-18310 (2013).
- 500 35. Lanore, F., *et al.* Deficits in morphofunctional maturation of hippocampal mossy fiber
501 synapses in a mouse model of intellectual disability. *J Neurosci* **32**, 17882-17893
502 (2012).
- 503 36. Tashiro, A., Dunaevsky, A., Blazeski, R., Mason, C.A. & Yuste, R. Bidirectional
504 regulation of hippocampal mossy fiber filopodial motility by kainate receptors. A two-
505 step model of synaptogenesis. *Neuron* **38**, 773-784 (2003).
- 506 37. Engert, F. & Bonhoeffer, T. Dendritic spine changes associated with hippocampal long-
507 term synaptic plasticity. *Nature* **399**, 66-70 (1999).
- 508 38. Matsuzaki, M., *et al.* Dendritic spine geometry is critical for AMPA receptor expression
509 in hippocampal CA1 pyramidal neurons. *Nat Neurosci* **4**, 1086-1092 (2001).
- 510 39. Matsuzaki, M. Factors critical for the plasticity of dendritic spines and memory storage.
511 *Neurosci Res* **57**, 1-9 (2007).
- 512 40. Wang, Z., *et al.* Myosin Vb mobilizes recycling endosomes and AMPA receptors for
513 postsynaptic plasticity. *Cell* **135**, 535-548 (2008).
- 514 41. Lerma, J. Kainate receptor physiology. *Current opinion in pharmacology* **6**, 89-97
515 (2006).
- 516 42. Malenka, R.C. & Nicoll, R.A. Long-term potentiation--a decade of progress? *Science*
517 **285**, 1870-1874 (1999).
- 518 43. Ylinen, A., *et al.* Sharp wave-associated high-frequency oscillation (200 Hz) in the
519 intact hippocampus: network and intracellular mechanisms. *J Neurosci* **15**, 30-46
520 (1995).

- 521 44. O'Neill, J., Senior, T. & Csicsvari, J. Place-selective firing of CA1 pyramidal cells during
522 sharp wave/ripple network patterns in exploratory behavior. *Neuron* **49**, 143-155
523 (2006).
- 524 45. Ego-Stengel, V. & Wilson, M.A. Disruption of ripple-associated hippocampal activity
525 during rest impairs spatial learning in the rat. *Hippocampus* **20**, 1-10 (2010).
- 526 46. Kato, H.K., Kassai, H., Watabe, A.M., Aiba, A. & Manabe, T. Functional coupling of the
527 metabotropic glutamate receptor, InsP3 receptor and L-type Ca²⁺ channel in mouse
528 CA1 pyramidal cells. *J Physiol* **590**, 3019-3034 (2012).
- 529 47. Miyazaki, K. & Ross, W.N. Ca²⁺ sparks and puffs are generated and interact in rat
530 hippocampal CA1 pyramidal neuron dendrites. *J Neurosci* **33**, 17777-17788 (2013).
- 531 48. Crepel, V. & Mulle, C. Physiopathology of kainate receptors in epilepsy. *Current*
532 *opinion in pharmacology* **20**, 83-88 (2015).
- 533 49. Motazacker, M.M., *et al.* A defect in the ionotropic glutamate receptor 6 gene (GRIK2)
534 is associated with autosomal recessive mental retardation. *American journal of human*
535 *genetics* **81**, 792-798 (2007).
- 536 50. Petrovic, M.M., *et al.* Inhibition of post-synaptic Kv7/KCNQ/M channels facilitates long-
537 term potentiation in the hippocampus. *PLoS One* **7**, e30402 (2012).

538

539

540

541

542

543

544

545

546

547

548

549 **Figure Legends**

550

551 **Fig 1. KA increases AMPAR surface expression.**

552 **A**, Immunoblots show the KA-evoked increased surface expression of GluA1 and GluA2,
553 which was blocked by CNQX. Data were quantified as % of control, n=3 independent
554 experiments. Dot-plots on the right indicated values for the individual experiments. Unless
555 otherwise indicated, all imaging and biochemistry experiments are performed in the
556 continuous presence of TTX (0.5 μ M), GYKI53655 (40 μ M) and L689560 (5 μ M).

557 **B**, Confocal images showing surface GluA1 and GluA2 in the dendritic shaft and spine (scale
558 bar 1 μ m) and cumulative frequency plots of spine/dendrite ratios. n=11-16 cells per
559 condition, 3 independent experiments.

560 **C**, Co-localization of GluA1 or GluA2 (red) and PSD95 (green). Scale bar 1 μ m. Graphs
561 show Pearson's coefficients for the co-localization. The black line in the whisker plot boxes
562 indicates the median. n=10-15 cells per condition, 3 independent experiments.

563 **D**, mEPSCs from CA1 pyramidal cells in hippocampal slices in the continuous presence of
564 APV and \pm GYKI and \pm KA. Quantification of the data using cumulative distribution plots of
565 mEPSC amplitudes and whisker plots. n=4 cells for control, n=5 cells for KA from n=4
566 animals.

567 In all experiments shown in B, C and D, data acquisition and analysis were performed in
568 blind with respect to the treatment.

569

570 **Fig 2. KAR activation induces LTP.**

571 **A**, Effects of KA on normalized evoked EPSC amplitudes and sample traces from CA1
572 neurons in the presence of D-APV in mice hippocampal slices. n=5 cells from 5 animals for
573 control and n=6 cells from 6 animals for kainate.

574 **B-C**, Schematic representations of the HFS and the RL-LTP induction protocols.

575 **D**, Normalized fEPSP slope in WT and GluK2^{-/-} mice subjected to RL-LTP. The symbols for
576 experiments without APV are squares (black for control and white for test pathway), whereas
577 for experiments with APV the symbols are circles (black for control and white for test
578 pathway). Arrow indicates point of RL-LTP stimulation. WT: n=8 slices from 8 animals; WT +
579 AP5: n=9 slices from 3 animals; GluK2^{-/-}: n=8 slices from 8 animals; GluK2^{-/-} + AP5 n= 8
580 slices from 8 animals.

581 **E**, Representative traces for D.

582 **F**, Normalized fEPSP slope values 21-30 min post LTP protocol.

583 In all experiments shown in B, C and D, data acquisition and analysis were performed in
584 blind with respect to the treatment or genotype of the animal.

585

586 **Fig 3. KAR-LTP induces structural plasticity.**

587 **A**, KAR-induced increase in spine size. Right panel shows quantification of spine area after
588 KA (A) / area before KA (A_0) versus time. The period of KA application is indicated by the
589 black bar. n=4-6 cells per condition, 3 independent experiments, Scale bars 1 μ m.

590 **B-C**, Time-lapse experiments showing KA-induced increase in the number of protrusions and
591 enhanced transition from stubby to mushroom spines. The number of protrusions was
592 quantified before KA application (N_0) and at the indicated times (N) in 10 μ m segments of
593 dendrites \pm KA. The period of KA application is indicated by the black bar. n=3-6 cells per
594 condition, 3 independent experiments. Scale bars 4 μ m.

595 In all experiments, data analysis was performed in blind with respect to the treatment.

596

597 **Fig 4. KAR-LTP recruits rab11-recycling endosomes to spines.**

598 **A**, KA (red arrow) recruits transferrin-Alexa594 (red) labelled recycling endosomes to spines.
599 GFP was expressed to visualise morphology. Time is indicated in seconds. Right panel
600 shows the quantification of the proportion of endosomes in head or shaft, n=5-6 cells per
601 condition, 3 independent experiments. Scale bar 1 μ m.

602 **B**, Dominant negative Rab11 prevents recruitment of recycling endosomes into spines. Tf-
603 A488 positive endosomes (green) in neurons expressing RFP-rab11wt or dn (red). n=6-8
604 cells per condition, 3 independent experiments. Scale bar 1 μ m.

605 **C**, Images of spines before (t=0) and 30 min (t=30) after KA +/- CNQX in neurons expressing
606 GFP, Rab11wt or Rab11dn. Frequency distribution plots of individual spine diameters before
607 (black, t=0) and after (grey dotted line, t=30 min) KA. n=4-5 cells per condition, 3
608 independent experiments. Scale bar 1 μ m.

609 In all experiments, data analysis was performed in blind with respect to the treatment.

610

611 **Fig 5. KAR-LTP requires intracellular calcium increase, PKC and PLC activation.**

612 **A-B**, BAPTA-AM, U73122 and chelerythrine, but not EDTA, block KAR-mediated increase in
613 co-localization of surface GluA1 or GluA2 (red) and PSD95 (green). Scale bar 1 μ m. Box-

614 and-whisker plots show range of Pearson's coefficient of controls (see also Supplementary
615 Fig. 5) and KA treated cells (KA). Black line in the boxes indicates the median. n=6-15 cells
616 per condition, 3 independent experiments. Data analysis was performed in blind with respect
617 to the pharmacological treatment.

618 **C**, Images of spines before (t=0) and 30 min (t=30) after indicated drugs +/- KA.
619 Corresponding graphs on the right show frequency distribution of individual spine diameters
620 before (black, t=0) and after (grey dotted line, t=30 min) KA. n=4 cells per condition, 3
621 independent experiments. Note that extracellular chelation of calcium by EDTA does not
622 prevent KAR-mediated increase in structural plasticity. Data analysis was performed in blind
623 with respect to the pharmacological treatment.

624 **D-E**, Effects of KA on normalized evoked EPSC amplitudes and sample traces from CA1
625 neurons in the presence of chelerythrine (upper panel) or the PLC inhibitor U-73122 (bottom
626 panel) in mice hippocampal slices. n=6 slices from 2 animals for chelerythrine and n=7 slices
627 from 2 animals for U-73122.

628 **F**, Box-and-whisker plots show range of fold increase in PLC (right) and PKC (left) activity
629 after KA challenge. PLC or PKC activity was normalized to controls in the presence of the
630 indicated drugs. Black line in the boxes indicates the median. n=4-6 independent
631 experiments.

632

633 **Fig 6. KAR-LTP requires KAR metabotropic signalling.**

634 **A**, Box-and-whisker plots show range of fold increase in PLC (right) and PKC (left) in cells
635 preincubated with PTX. PLC or PKC activity was normalized to control and performed in
636 parallel with the experiment in figure 5C. Black line in the boxes indicates the median. n=4-6
637 independent experiments.

638 **B**, Co-localization of surface GluA1 or GluA2 (red) and PSD95 (green). Scale bar 1 μ m. Box-
639 and-whisker plots of Pearson's coefficients of colocalization indicate that the metabotropic
640 pathway inhibitor PTX blocks KAR-evoked increase in surface AMPARs. Black line in the
641 boxes indicates the median. n=9-13 cells per condition, 3 independent experiments.

642 **C**, PTX blocks KAR-mediated increase in CA1 mEPSC amplitude (compare to Fig. 1D). n=3
643 cells from 3 animals. Examples of traces pretreated with PTX before and after GYKI53655
644 (control) and shown before and after KA plus GYKI53655 (KA+GYKI). Graphs show
645 cumulative frequency distribution of mEPSC amplitudes and box-and-whisker plots in insets
646 indicating range.

647 **D**, Preincubation with PTX impaired the KA-induced increase of normalized evoked EPSC
648 amplitudes in WT mice hippocampal slices (compare with Fig. 2A). Sample traces are shown
649 before and after KA challenge. n=6 cells from 3 animals per condition.

650 **E**, Normalized fEPSP slope recorded in WT-mice hippocampal slices pretreated with PTX.
651 Arrow indicates point of LTP induction. n=7 slices from 4 animals.

652 **F**, Images of spines before (t=0) and 30 min (t=30) after KA in cells treated with PTX.
653 Frequency distribution of individual spine diameters before (black, t=0) and after (red, t=30
654 min) KA. n=3 cells per condition, 3 independent experiments.

655 In all experiments data analysis was performed in blind with respect to the treatment.

656

657 **Fig 7. KAR-LTP does not require ionotropic KAR activation.**

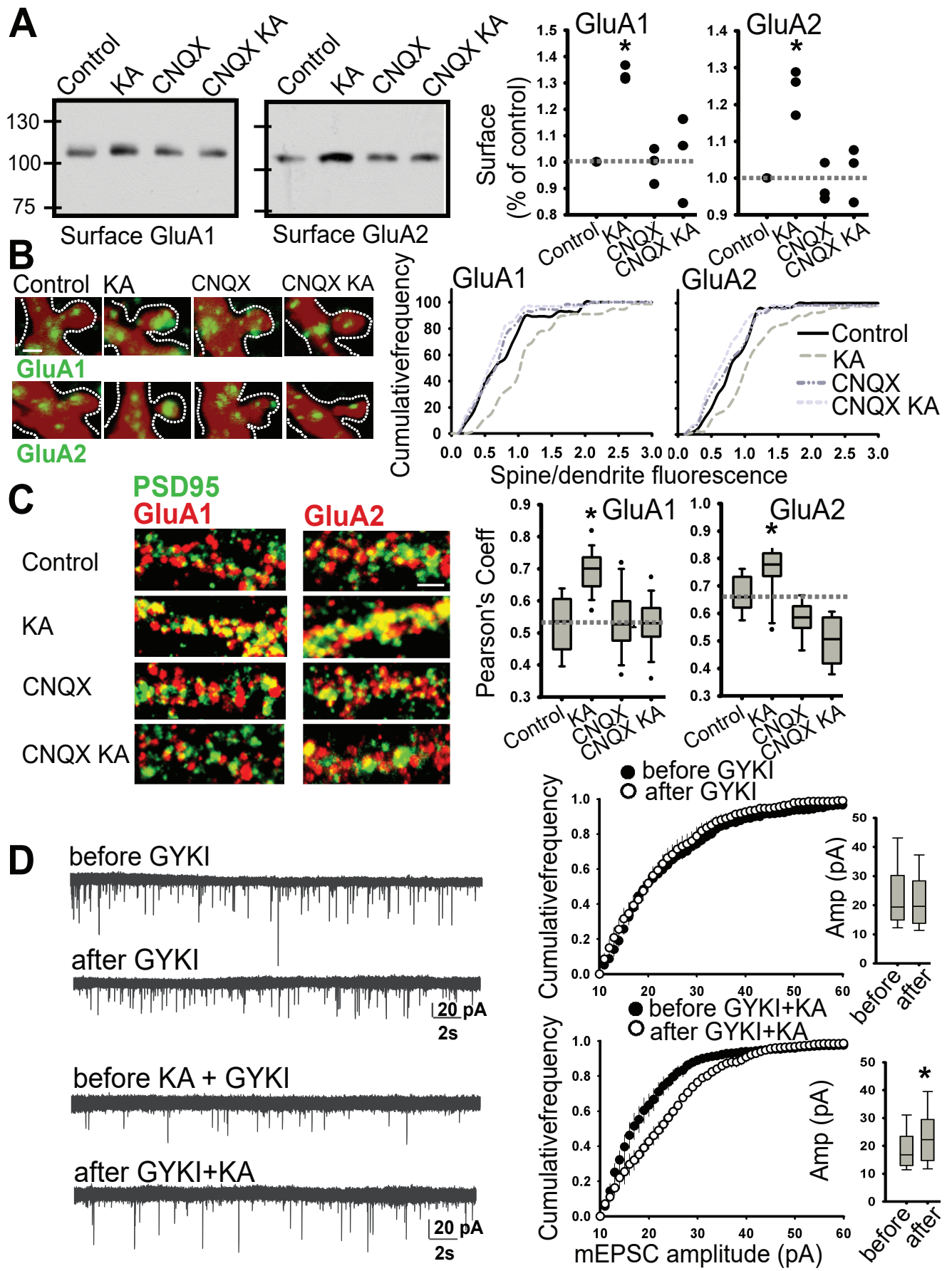
658 **A**, Box-and-whisker plots show fold increase in PLC (right) and PKC activity (left) in the
659 presence of the ionotropic KAR inhibitor UBP310 (10 μ M). PLC or PKC activity was
660 normalized to control and performed in parallel with the experiments in figure 5C. Black line
661 in the boxes indicates the median. n=6 independent experiments.

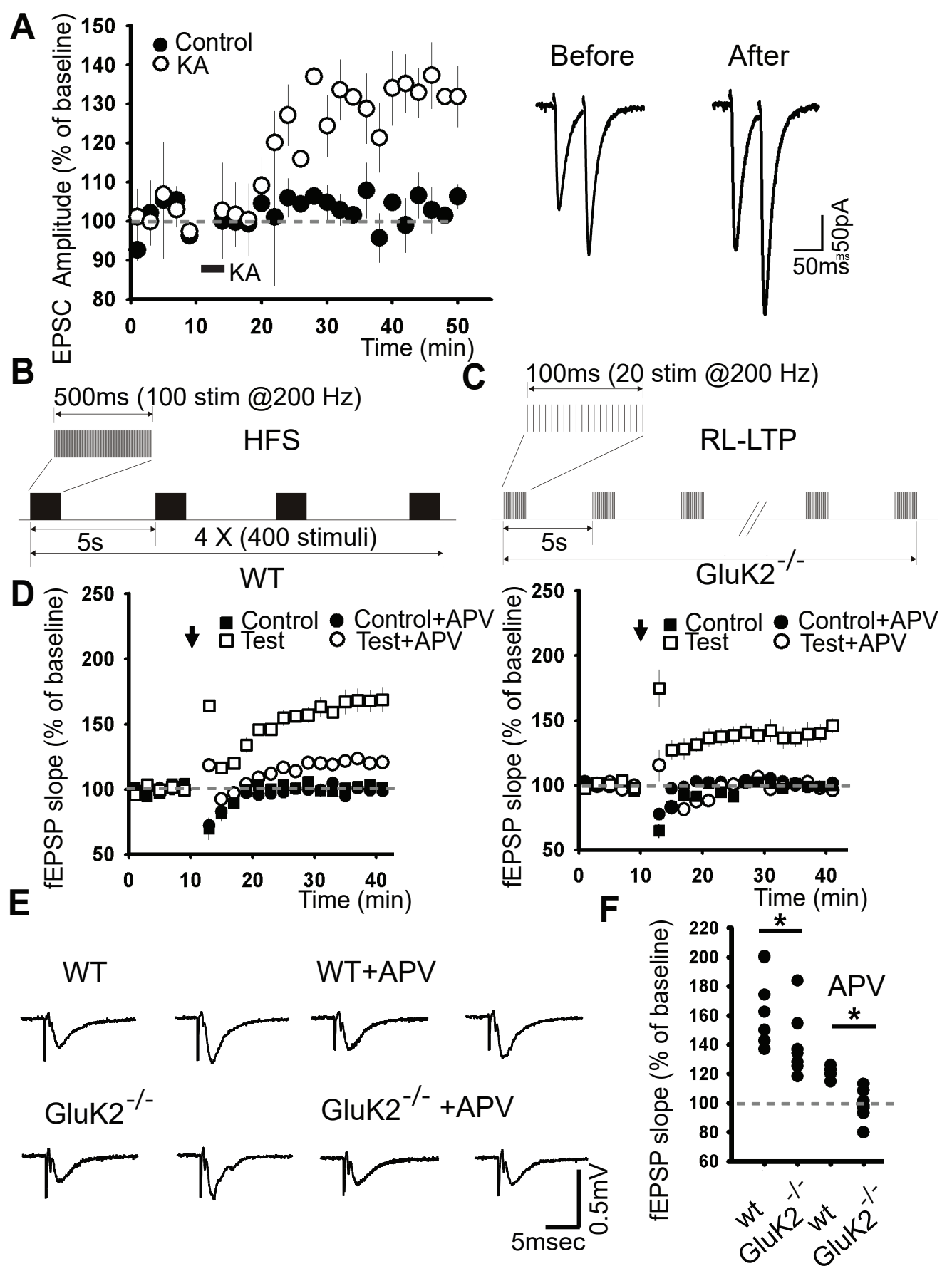
662 **B**, UBP310 (10 μ M) did not impair the KA-induced increase of normalized evoked EPSC
663 amplitudes in WT mice hippocampal slices (compare with Fig. 2A). Sample traces are shown
664 before and after KA challenge. n=5 cells from 4 animals.

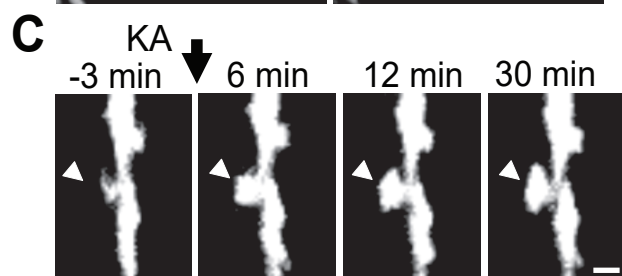
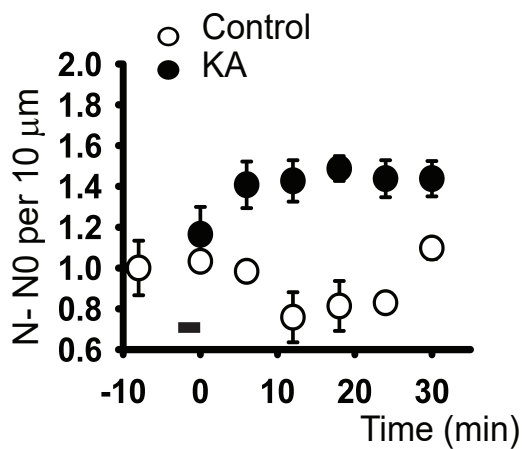
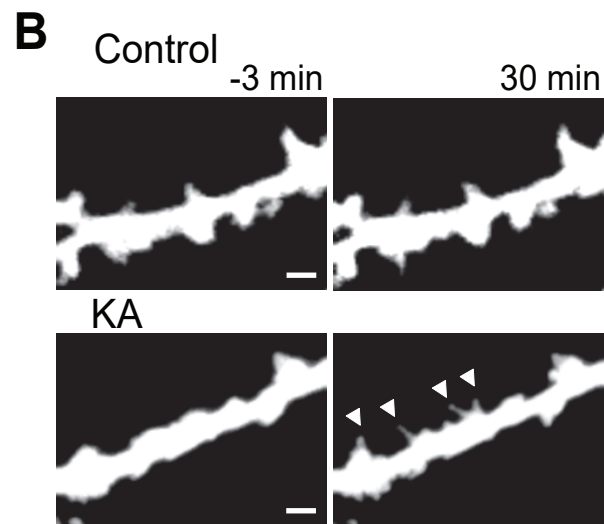
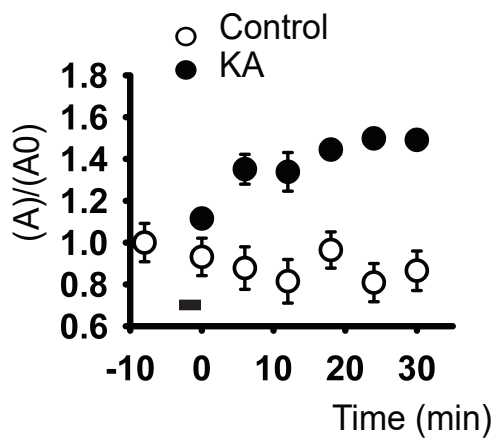
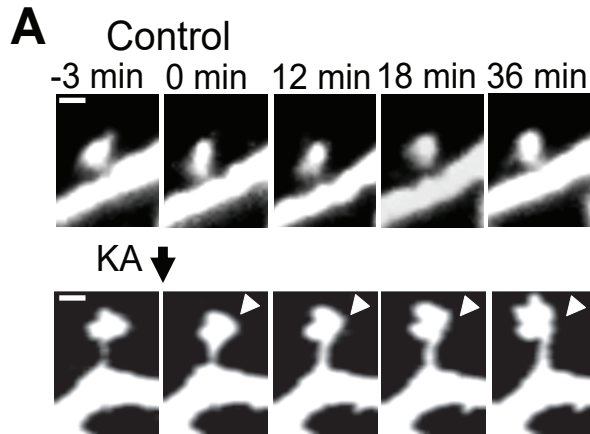
665 **C**, Normalized fEPSP slope recorded in WT mice hippocampal slices in the presence of
666 UBP310 (10 μ M). Arrow indicates time point of LTP induction. n=11 slices per condition from
667 6 animals.

668 **D**, Images of spines before (t=0) and 30 min (t=30) after KA in cells treated UBP310 (10 μ M).
669 Frequency distribution of individual spine diameters before (black, t=0) and after (red, t=30
670 min) KA. n=4-6 cells per condition, 3 independent experiments. Data analysis was performed
671 in blind with respect to the pharmacological treatment.

672







	% Stubby to Mushroom
Control	-13.95±3
KA	18.75±4

* (indicates significant difference between Control and KA)

